

EXPERIMENTAL VALIDATION OF AN ACCELERATION POWER SPECTRAL DENSITY AIRCRAFT PANEL MODEL GIVEN DIFFERENT EXCITATIONS

Steven A.J. Sonnenberg ^{*1}, Joana Rocha ^{†1}, Malte Misol ^{‡2} et Michael Rose ^{♦2}

¹Department of Mechanical and Aerospace Engineering, Carleton University, Ottawa, Ontario, Canada.

²DLR-Institut für Faserverbundleichtbau und Adaptronik, Braunschweig, Deutschland.

Résumé

Le bruit et les vibrations dans une cabine d'avion pendant les conditions de croisière sont principalement causés par des excitations d'écoulement externes provenant de la couche limite turbulente (TBL). Le TBL fait vibrer les panneaux de fuselage de l'avion. Ces vibrations rayonnent l'énergie sonore sous la forme de bruit. Il est intéressant de pouvoir prédire la réponse de ces panneaux à différentes excitations à l'aide d'un modèle analytique, de sorte que les essais coûteux en soufflerie et en vol puissent être minimisés lors de la recherche sur le bruit. Deux modèles analytiques existants ont été modifiés pour tenir compte des différentes excitations: l'une avec des conditions aux limites simplement supportées et l'autre avec des conditions aux limites arbitraires. Ces modèles ont été programmés et validés par rapport à des données expérimentales, obtenues par les auteurs, pour un panneau mince rectangulaire avec des conditions aux limites entre des conditions simplement supportées et des conditions serrées. Le but de cette recherche est d'utiliser les modèles pour mener des études d'optimisation, simuler expérimentalement la réponse vibratoire résultante sur un panneau soumis à des fluctuations de pression TBL et utiliser un patch piézo-électrique pour simuler expérimentalement la même réponse de panel à partir d'un TBL excitation. On montre que les modèles analytiques modifiés prédisent avec précision la réponse du panneau pour une excitation de force ponctuelle, pour une excitation TBL et pour une excitation de patch piézoélectrique oscillant.

Mots clefs : couche limite turbulente, modèle analytique, densité spectrale de puissance, acoustique structurale, aéroacoustique

Abstract

The noise and vibration in an aircraft cabin during cruise conditions is primarily caused by external flow excitations from the turbulent boundary layer (TBL). The TBL causes the fuselage panels on the aircraft to vibrate. These vibrations radiate sound energy in the form of noise. It is of interest to be able to predict the response of these panels to different excitations using an analytical model, so that expensive wind tunnel and flight tests can be minimized when doing noise research. Two existing analytical models were modified to account for different excitations: one with simply supported boundary conditions and the other with arbitrary boundary conditions. These models were programmed and validated against experimental data, obtained by the authors, for a thin rectangular panel with boundary conditions between simply supported and clamped conditions. The goal of this research is to use the models to conduct optimization studies, experimentally simulate the resulting vibration response on a panel subjected to TBL pressure fluctuations and to use a piezo-electric patch as a means of experimentally simulating the same panel response from a TBL excitation. It is shown that the modified analytical models accurately predict the panel response for a point force excitation, for a TBL excitation, and for an oscillating piezoelectric patch excitation.

Keywords: turbulent boundary layer, analytical model, power spectral density, structural acoustics, aeroacoustics

1 Introduction

The noise and vibration in an aircraft cabin during cruise conditions is primarily caused by the external turbulent boundary layer (TBL) [1]. The TBL causes the fuselage panels on the aircraft to vibrate, which radiate sound energy in the form of noise in the cabin. In this context, the objective of this study is to validate an analytical model which predicts the behaviour of an aircraft panel, subject to

different excitations, and with simply supported and arbitrary boundary conditions. The model will be given 1) a point force excitation from an impact hammer, 2) a turbulent boundary layer excitation caused by the flow on the outside of the panel, and 3) an excitation from a piezoelectric actuator bonded to the panel. The theoretical values, as predicted by the model, are then validated against experimental data for the three excitations.

Many researchers have studied the prediction of the response of a simple panel due to the TBL. Strawderman and Brand have some of the earliest simulated results for a turbulent flow excited panel vibration [2]. Others have modelled the response of the plate using wavenumber-frequency formulations, or have used finite element and

* Steven.Sonnenberg@carleton.ca

† Joana.Rocha@carleton.ca

‡ Malte.Misol@dlr.de

♦ Michael.Rose@dlr.de

boundary element methods where the plate is excited by a number of distributed forces having proper spatial and temporal correlations [3–6]. These methods tend to be very computationally intensive and as such are not a suggested approach when using recursive optimization routines or control algorithms, which are often involved in the reproduction of these types of responses. These types of models tend to be very robust for a variety of complex experimental conditions however, this makes them overanalyze simplified experimental conditions causing more calculations to be performed per iteration of an optimization routine.

One approach to calculate the radiated sound power (RSP) of vibrating structures is to use a modal analysis, as done by Roy and Lapi [7]. This approach is necessary when analyzing obscure shapes, but requires great computational power and time, making it difficult to iterate the calculations for optimization routines. Therefore, when looking at simple shapes, like that of a flat panel, analytical computational methods become a better choice. The analytical expressions for RSP can be derived for a given aircraft panel in terms of the displacement power spectral density (PSD) [1,8,9]. The acceleration PSD is calculated from the displacement PSD, which is proportional to the RSP [9]. The analytical models previously developed by Rocha were modified to account for other panel and enclosure combinations [10,11]. Berry also showed that the same type of analytical analysis was possible for panels with arbitrary boundary conditions [12]. Other studies have attempted to reproduce the TBL excitation using loudspeakers [13–19]. It was found that at low frequencies accurate reproduction can be obtained, however, the higher the frequency range the more loudspeakers are required and the more complex the control signals become. It has been predicted that using piezoelectric patches to excite the panel might require less actuators than loud speakers to obtain the same quality of reproduction at low frequencies and it might allow the response to be reproduced for higher frequency ranges because it removes the air gap in between the excitation device and the panel [20]. Piezoelectric patches also come in varying sizes allowing more to be bonded to the panel then the amount of loudspeakers that can be arranged in front of the panel. This is an additional reason why it is of great importance in this paper to prove that an accurate model exists for a panel with an excitation from a piezoelectric patch.

There have been many experimental setups used to try to replicate an aircraft panel. Some have attempted to reproduce a panel with simply supported boundary conditions, which allows the equations for the acceleration PSD response to be simplified [21–25]. However, these experimental setups are either very difficult to manufacture or are structurally weak for a thin aircraft panel. Additionally, a true aircraft panel, which were assumed to be simply supported for most of the tests outlined in this paper, are not actually simply supported as they often have boundary conditions in between simply supported and clamped conditions. Therefore, the experimental setup used

to validate Berry’s model for arbitrary boundary conditions is the one used at DLR for their experimental work [19,26].

2 Methodology

Two main models have been used in this study, and further modified to account for different excitations. These are Rocha’s Model and Berry’s Model. Rocha’s Model is an analytical approach for a panel with simply supported boundary conditions and uses trigonometric spatial functions [1,8–11]. Berry’s Model is developed for a panel with arbitrary boundary conditions and uses polynomial spatial functions [12,27]. The following section describes briefly each model and different excitations used.

2.1 Rocha’s model

In this model, the panel is assumed to be flat and simply supported on all four sides. A panel, in the context of an aircraft, might not be defined as the boundary of a sheet of material, but instead as the enclosed area on that sheet, between the stringers and the formers. The connections of the material to the stringers and formers cause that section of material to act as a single, simply supported panel. The vibration of a single panel can be defined as [1]:

$$w(x, y, t) = \sum_{m_x=1}^{M_x} \sum_{m_y=1}^{M_y} \alpha_{m_x}(x) \beta_{m_y}(y) q_{m_x m_y}(t) \quad (1)$$

In which α_{m_x} and $\beta_{m_y}(y)$ are spatial functions that define the variation in vibration and can be defined as follows, for a simply supported plate [1]:

$$\alpha_{m_x}(x) = \sqrt{\frac{2}{a}} \sin\left(\frac{m_x \pi x}{a}\right); \beta_{m_y}(y) = \sqrt{\frac{2}{b}} \sin\left(\frac{m_y \pi y}{b}\right) \quad (2)$$

Rocha’s research is able to reduce a “coupled system governing equations into the following matrix form” [1]:

$$\begin{bmatrix} M_{pp} & 0 \\ M_{cp} & M_{cc} \end{bmatrix} \begin{Bmatrix} \ddot{q}(t) \\ \ddot{r}(t) \end{Bmatrix} + \begin{bmatrix} D_{pp} & 0 \\ 0 & D_{cc} \end{bmatrix} \begin{Bmatrix} \dot{q}(t) \\ \dot{r}(t) \end{Bmatrix} + \begin{bmatrix} K_{pp} & K_{pc} \\ 0 & K_{cc} \end{bmatrix} \begin{Bmatrix} q(t) \\ r(t) \end{Bmatrix} = \begin{Bmatrix} P_{tbl}(\omega) \\ 0 \end{Bmatrix} \quad (3)$$

Where pp is used to denote the panel cc is to denote the enclosure and cp and pc are the interactions between the panel and enclosure. $q(t)$ defines the variation in $w(x, y, t)$ with respect to time and $r(t)$ is similarly defined for the enclosure. This matrix form assumes that the panel is simply supported, and encloses a cavity (like the panels surrounding the enclosed cabin of the aircraft). In this study, the author will assume that the cavity is not present and therefore the system equations can be reduced to:

$$H_w(\omega) = H(\omega) = [-\omega^2 M_{pp} + i\omega D_{pp} + K_{pp}]^{-1} \quad (4)$$

Where [1]:

$$M_{pp} = \text{diag}[\rho_p h_p] \quad (5)$$

$$D_{pp} = \text{diag}[2\rho_p h_p \omega_m \zeta_p] \quad (6)$$

$$K_{pp} = \text{diag}[\rho_p h_p \omega_m^2] \quad (7)$$

Each of these matrices are of size MxM. With this information, $S_{ww}(\omega)$ matrix can be defined as follows [1]:

$$S_{ww}(\omega) = H_w^*(\omega) S_e(\omega) H_w^T(\omega) \quad (8)$$

In this equation, $S_e(\omega)$ is a generalized PSD matrix of the different excitations. The * operator is used to denote the Hermitian conjugate and the T operator indicates the transpose of the matrix. With this displacement PSD matrix, the displacement PSD at a single point can be calculated for a given frequency as follows [1]:

$$S_{WW}(x_1, y_1, x_2, y_2, \omega) \quad (9)$$

$$= \sum_{m_{x_1}, m_{x_2}=1}^{M_x^2} \sum_{m_{y_1}, m_{y_2}=1}^{M_y^2} \alpha_{m_{x_1}}(x_1) \alpha_{m_{x_2}}(x_2) \beta_{m_{y_1}}(y_1) \beta_{m_{y_2}}(y_2) S_{ww}(\omega)_{m_1, m_2}$$

When $x_1 = x_2$ and $y_1 = y_2$ this calculates the autocorrelation at a single point and if these are not equal than it calculates the cross spectrum correlation between two different points. For the TBL excitation the autocorrelation is used and for the point force and the piezoelectric patch excitations the cross spectrum correlation is used. The equations required to calculate the velocity (S_{VV}) and the acceleration PSD (S_{AA}), at a single point on the panel are as follows [9]:

$$S_{VV} = \omega^2 S_{WW} \quad (10)$$

$$S_{AA} = \omega^4 S_{WW} \quad (11)$$

More information regarding Rocha's Model can be found in Appendix A.

2.2 Berry's model

The vibration of a single panel can still be defined as in equation (1), however, as Berry shows, the spatial functions used can be changed to polynomial functions [12].

$$\alpha_{m_x}(x) = \frac{2}{a} x^{m_x}; \beta_{m_y}(y) = \frac{2}{b} y^{m_y} \quad (12)$$

A difference between the two methods is that Berry's model treats the panel mode indices as if they start at 0 instead of starting at 1. Similarly to equation (4), Berry defines the equation as follows [12]:

$$(-\omega^2 M_{mnpq} + \tilde{K}_{mnpq}) \{a_{mn}\} = \{f_{mn}\} \quad (13)$$

Where:

$$mnpq = m_{x_1} m_{y_1} m_{x_2} m_{y_2} \text{ and } a_{mn} = q_{m_x m_y}$$

a_{mn} is solved in equation (13) and is used to calculate the displacement PSD of the panel as follows:

$$w(x, y, \omega) = \sum_{m=1}^{M_x} \sum_{n=1}^{M_y} \alpha_m(x) \beta_n(y) a_{mn} \quad (14)$$

$$S_{ww}(\omega) = w(x, y, \omega) w(x, y, \omega)^* \quad (15)$$

2.3 Panel excitations and modified berry's model

For both of the models used, it is important to determine the correct way to represent the excitation. Rocha's model uses the excitation in its PSD form, whereas Berry's Model treats the excitation as a force spectrum. An impulse force can be represented as follows:

$$S_e(\omega) = f_{mn}(\omega) f_{mn}(\omega)^* \quad (16)$$

$$f_{mn}(\omega) = \alpha_m(x) \beta_n(y) f(\omega) \quad (17)$$

Here $f(\omega)$ is the frequency response of the force input as measured by the impact hammer. The spatial functions and mode numbering conventions change between the two models. However, using an impact force is the simplest excitation for both models.

The excitation from a TBL on the plate has previously been defined for Rocha's model. This work investigates the use of Rocha's model, for the TBL excitation, but using polynomial spatial functions [1]. An analytical equation has been defined for use with Berry's model of a TBL excitation with polynomial spatial functions. The following is the result of this derivation: the derivation starts with the Corcos model, which considers the cross power spectral density of the stationary and homogeneous turbulent boundary layer wall pressure field in a separable form in the streamwise, x-, and spanwise, y-directions, as follows [28,29]:

$$S(\zeta_x, \zeta_y, \omega) \quad (18)$$

$$= S_{ref}(\omega) e^{-\frac{\alpha_x \omega |\zeta_x|}{U_c}} e^{-\frac{\alpha_y \omega |\zeta_y|}{U_c}} e^{-i \frac{\omega \zeta_x}{U_c}}$$

Therefore the power spectrum from a turbulent boundary layer is defined as:

$$S_{tbl}(\omega) = \iint_{y_0}^{y_1} \iint_{x_0}^{x_1} \Phi_m(x) \varphi_n(y) \Phi_p(x') \varphi_q(y') S(\zeta_x, \zeta_y, \omega) dx dy dx' dy' \quad (19)$$

Where the spatial separations in the streamwise and spanwise directions are $\zeta_x = x - x'$ and $\zeta_y = y - y'$. The polynomial spatial functions can be defined as:

$$\Phi_m(x) = \alpha^m; \varphi_n(y) = \beta^n \quad (20)$$

Where:

$$-1 \leq \alpha, \beta \leq 1 \text{ and } \alpha = \frac{2x}{a}; \beta = \frac{2y}{b} \quad (21)$$

After substituting equation (18) and the polynomial spatial functions into (19) the following results:

$$\frac{S_{tbl}(\omega)}{S_{ref}(\omega)} = \iint_{x_0}^{x_1} \alpha^m \alpha'^p e^{-\frac{\alpha_x \omega |\zeta_x|}{U_c}} e^{-i\frac{\omega \zeta_x}{U_c}} dx dx' \quad (22)$$

$$\iint_{y_0}^{y_1} \beta^n \beta'^q e^{-\frac{\alpha_y \omega |\zeta_y|}{U_c}} dy dy'$$

Let:

$$x_0 = \frac{a}{2} \alpha_0; \quad x_1 = \frac{a}{2} \alpha_1; \quad (23)$$

$$y_0 = \frac{b}{2} \beta_0; \quad y_1 = \frac{b}{2} \beta_1;$$

And $-1 \leq \alpha_0, \alpha_1, \beta_0, \beta_1 \leq 1$ therefore:

$$\frac{S_{tbl}(\omega)}{S_{ref}(\omega)} \quad (24)$$

$$= \frac{a^2 b^2}{16} \iint_{\alpha_0}^{\alpha_1} \alpha^m \alpha'^p e^{-\frac{\alpha_x \omega a}{2U_c} |\alpha - \alpha'|} e^{-i\frac{\omega a}{2U_c} (\alpha - \alpha')}$$

$$d\alpha d\alpha' \iint_{\beta_0}^{\beta_1} \beta^n \beta'^q e^{-\frac{\alpha_y \omega b}{2U_c} |\beta - \beta'|} d\beta d\beta'$$

This can be simplified to:

$$S_{tbl}(\omega) = S_{ref}(\omega) \frac{a^2 b^2}{16} S_\alpha S_\beta \quad (25)$$

Let:

$$\mu = \frac{\alpha_x \omega a}{2U_c}; \quad \kappa = \frac{\omega a}{2U_c}; \quad \rho = \frac{\alpha_y \omega b}{2U_c} \quad (26)$$

Therefore:

$$S_\alpha = \int_{\alpha_0}^{\alpha_1} \alpha^m e^{-(\mu+i\kappa)\alpha} \int_{\alpha_0}^{\alpha} \alpha'^p e^{(\mu+i\kappa)\alpha'} d\alpha' d\alpha \quad (27)$$

$$+ \int_{\alpha_0}^{\alpha_1} \alpha^m e^{(\mu-i\kappa)\alpha} \int_{\alpha}^{\alpha_1} \alpha'^p e^{-(\mu-i\kappa)\alpha'} d\alpha' d\alpha$$

$$= S_L + S_U$$

With a change of variables:

$$S_\beta \cong S_\alpha \quad (28)$$

This occurs when $\alpha_0 \rightarrow \beta_0, \alpha_1 \rightarrow \beta_1, \mu \rightarrow \rho, \kappa \rightarrow 0, \alpha \rightarrow \beta$ and $\alpha' \rightarrow \beta'$. Further simplifying of these equations by setting $z = \mu + i\kappa$ leads to:

$$S_L = \int_{\alpha_0}^{\alpha_1} \alpha^m e^{-z\alpha} \int_{\alpha_0}^{\alpha} \alpha'^p e^{z\alpha'} d\alpha' d\alpha \quad (29)$$

$$S_U = \int_{\alpha_0}^{\alpha_1} \alpha^m e^{\bar{z}\alpha} \int_{\alpha}^{\alpha_1} \alpha'^p e^{-\bar{z}\alpha'} d\alpha' d\alpha \quad (30)$$

$$S_U = \int_{\alpha_0}^{\alpha_1} \alpha'^p e^{-\bar{z}\alpha'} \int_{\alpha_0}^{\alpha} \alpha^m e^{\bar{z}\alpha} d\alpha d\alpha' \quad (31)$$

With a change of variables: $m \rightarrow p$ and $z \rightarrow \bar{z}$ then $S_U \cong S_L$. These equations can then be integrated to result in an analytical expression where $S_L = f_{m,p}$:

$$f_{m,p} = \frac{1}{z} \left[m f_{m-1,p} - \alpha_1^m e^{-z\alpha_1} g_p + \frac{\alpha_1^{m+p+1} - \alpha_0^{m+p+1}}{m+p+1} \right] \quad (32)$$

$$g_p = \frac{1}{z} [\alpha_1^p e^{z\alpha_1} - \alpha_0^p e^{z\alpha_0} - p g_{p-1}] \quad (33)$$

Where: $m, p \geq 0$ and $f_{-1,p} = 0$ and $g_{-1} = 0$

The piezoelectric actuator excitation has previously been defined for Berry's Model by Charette and Berry [27]. It treats the force from the piezoelectric patch as a point force located at its center. It shows how to incorporate the effects of the piezoelectric patch to the mass and stiffness matrices of the panel. These values often have very little effect on large panels due to the relative size of a single patch. However, it is important to include the patches impact in the model because the authors aim to modify the model to include multiple patches at different locations, which will have a more significant impact on the panels' mass and stiffness matrices. One major deviation in this work from Charette's paper, is that instead of using a piezoelectric patch on both sides of the panel it has only been used on one side. Therefore the equations defined are all divided by two.

3 Results

3.1 Impact hammer

The first goal was to use the impact hammer to strike the panel at one location and measure the acceleration using an accelerometer at a different location on the panel. The benefit of this test is that it is accurate and relatively simple to complete multiple configurations of hammer and accelerometer locations.

The first step was to compare Rocha's model to Berry's model. Therefore, boundary conditions of a simply supported panel were used in Berry's model and the same panel parameters were given to each code. Table 1 lists the panel parameters of the test panel used and Figure 1 shows

the resulting acceleration PSD for a given impact excitation for each of the models and compares it to simulation results obtained from Ansys. The Ansys results were obtained from the same model defined previously by Misol using shell elements for the plate and torsional springs to describe the fixture at the edges [19]. Berry's model cannot accept infinity for the translational stiffness constant, therefore, a value of $5 * 10^7$ was used [12]. The goal of this work is to test for a single point acceleration PSD not the overall acceleration PSD. This work is to show the accuracy of both Berry's and Rocha's model at predicting the panel response and it is not required to check the overall response however, multiple tests at different random panel locations have been taken for each test.

Figure 1 shows the models predict the same general shape for the acceleration PSD for a given point force excitation. However, there are two main differences in the outputs of the models: 1) the magnitudes of the peaks are different and 2) at higher frequencies the models appear to not agree. The difference in magnitudes of the peaks is likely due to the way the damping is entered into each model. In Rocha's model the damping is defined using the damping matrix, whereas in Berry's model the effects of the panel's damping are included as an imaginary component in the stiffness matrix. This might be the reason why Berry's model underpredicts the amount of damping compared to Rocha's model and FEM results. The divergence of Berry's model occurs around 600 Hz due to the number of panel modes used at these high frequencies. Berry's model runs into the error of the matrix appearing singular when the mode number is high, $(m, n) \geq (10, 10)$. This error can be removed if frequencies of interest are small enough, or the panel's thickness is increased, requiring less panel modes. However, it appears that by selecting polynomial trial functions severely limits the frequency range that can be calculated.

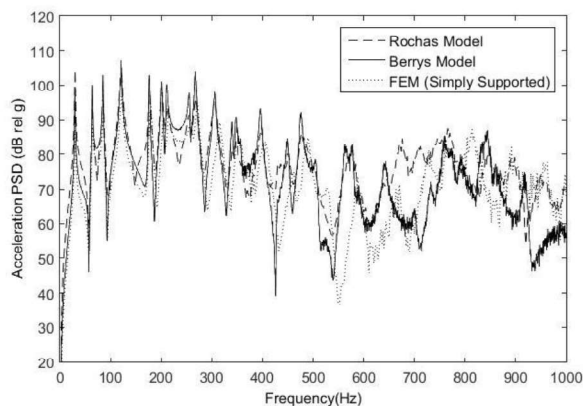


Figure 1: Comparison of acceleration PSD results for a panel with simply supported boundary conditions at a point $x = 20.6$ cm and $y = 21.6$ cm, with a point force applied at $x = 7.7$ cm and $y = 3.8$ cm for three different models.

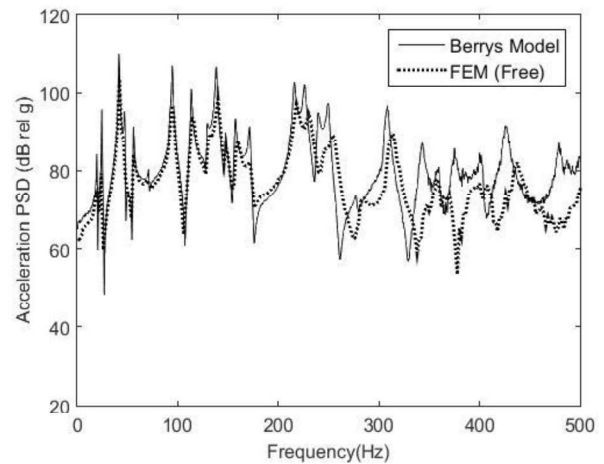


Figure 2: Comparison of acceleration PSD results for a panel with free boundary conditions at a point $x = 20.6$ cm and $y = 21.6$ cm with a point force applied at $x = 7.7$ cm and $y = 3.8$ cm for two different models.

Table 1: Physical properties of the test panel.

Variable	Description, Units	Value
a	Panel Length [m]	0.47
b	Panel Width [m]	0.37
ρ_p	Panel Density [kg m^{-3}]	2800
h_p	Panel Thickness [m]	0.0011
ν_p	Poisson Ratio	0.3
E_p	Panel Elasticity Modulus [Pa]	$6.5 * 10^{10}$
ζ_p	Damping Ratio	0.01
N_x	Panel Longitudinal Tension [Nm^{-1}]	0
N_y	Panel Lateral Tension [Nm^{-1}]	0

The next step was to check Berry's model given "free" boundary conditions. The rotational and translational stiffness constants were set to zero and the acceleration PSD at a single point was again compared to the results given from the Ansys model. The results can be seen in Figure 2. The third step was to gather experimental data. Using the test setup at DLR, an accelerometer was placed on the panel using wax, and the panel struck using an impact hammer [19,26]. The impact hammer location and accelerometer location were measured and both the force data and the acceleration data were recorded. The accelerometer data was used as the experimental PSD values and were compared to the results given by Berry's model using the force data from the impact hammer as the input to the model. This test enabled the translational and rotational stiffness constants (c and k) to be found for the test panel. This was done by varying the values of c and k until the predicted plot most accurately matched the experimental data, as seen in Figure 3. The DLR test panel with test locations (F for Force Applied and M for Acceleration Measurement locations) can be seen in Figure 4. Some of the test instrumentation mounted on the panel can be seen in Figure 5

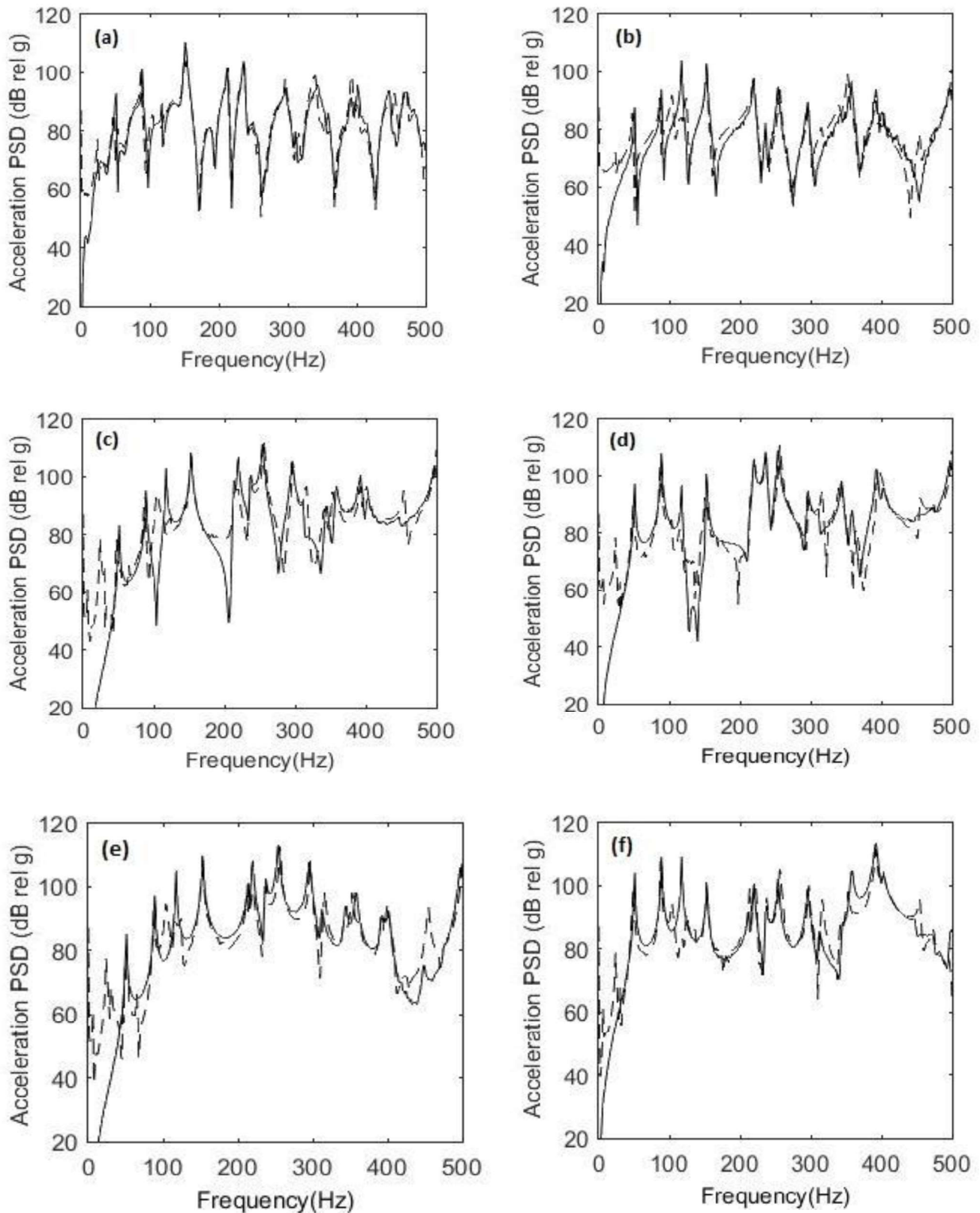


Figure 3: Comparison for predicted (solid line) vs. experimental (dashed line) of acceleration PSD results for a panel with arbitrary boundary conditions at: (a) measured at (M): $x = 5.4$ cm, $y = 13.6$ cm and force applied at (F): $x = 5.4$ cm and $y = 13.6$ cm, (b) M: $x = 31.2$ cm, $y = 32.1$ cm and F: $x = 31.2$ cm and $y = 32.1$ cm, (c) M: $x = 31.2$ cm, $y = 32.1$ cm and F: $x = 4.5$ cm and $y = 3.9$ cm, (d) M: $x = 31.2$ cm, $y = 32.1$ cm and F: $x = 4.2$ cm and $y = 19.8$ cm, (e) M: $x = 31.2$ cm, $y = 32.1$ cm and F: $x = 4.2$ cm and $y = 32.2$ cm, (f) M: $x = 31.2$ cm, $y = 32.1$ cm and F: $x = 10.6$ cm and $y = 26.0$ cm.

To ensure that the model was working accurately over the entire panel, 14 more hammer and accelerometer locations were measured experimentally. The experimental data was compared to the predicted values and they all resulted in similar plots. This indicated that the model worked over the entire area of the plate and that the values of c and k selected were accurate.

It is important to note that since Berry's model uses polynomial trial functions it takes many more modes to accurately predict the acceleration PSD than Rocha's model does. In the convergence equations, in order to get accurate predictions for Berry's model, F_{max} is set 5 times higher than when used for Rocha's model. This means it takes more modes to result in an accurate prediction of the acceleration PSD, being more computationally expensive.

3.2 TBL Excitation

To ensure the new derivation of a TBL excitation defined with polynomial spatial functions was correct, the results for Rocha's model and Berry's model were compared. Rocha's model has been previously verified compared to actual wind tunnel test data obtained at NASA, and this code has been validated against these results [1,30]. Berry's model was set with simply supported boundary conditions and run for the same flight conditions as Rocha's. Table 2 contains the flow conditions used to predict the TBL over the test panel. The results of this comparison can be found in Figure 6.

The accuracy of Berry's model given a TBL input is very sensitive to the number of panel modes used. Figure 7 and Figure 8 contain the results of using the same number of panel modes for each of the target frequencies. It shows that each target frequency requires a different number of panel modes to result in an accurate prediction of the acceleration PSD from a TBL excitation. They show that it is critical to make a preliminary study on Berry's model so reliable results can be obtained. These plots are limited to 400 Hz to highlight how sensitive Berry's model is to the number of panel modes used.

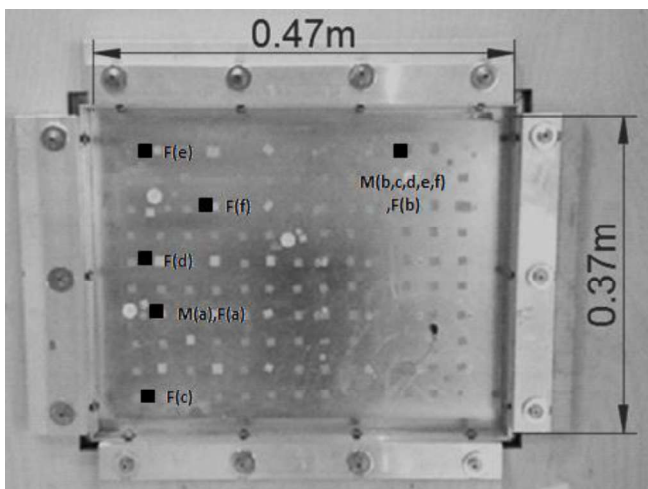


Figure 4: Front view of the DLR test setup with impact force test locations.

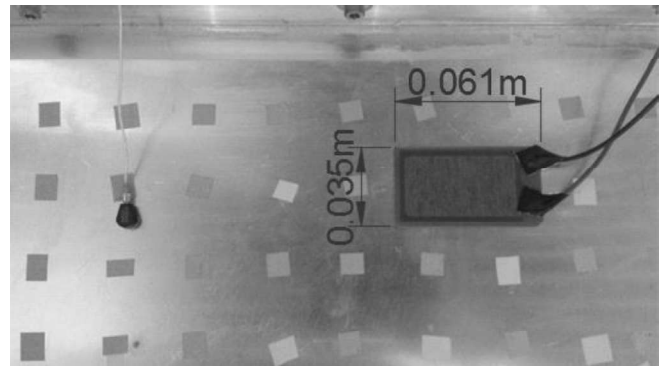


Figure 5: Excitation and monitoring system of the DLR test setup, using a piezoelectric patch and an accelerometer.

Table 2: Air parameters for determining TBL.

Variable	Description, Units	Value
ρ_0	Density of Air [kg m^{-3}]	1.225
c_0	Speed of Sound [m s^{-1}]	340
U_i	Freestream Velocity [m s^{-1}]	35.8
U_c	Convective Velocity [m s^{-1}]	23.3
M	Mach Number	0.105

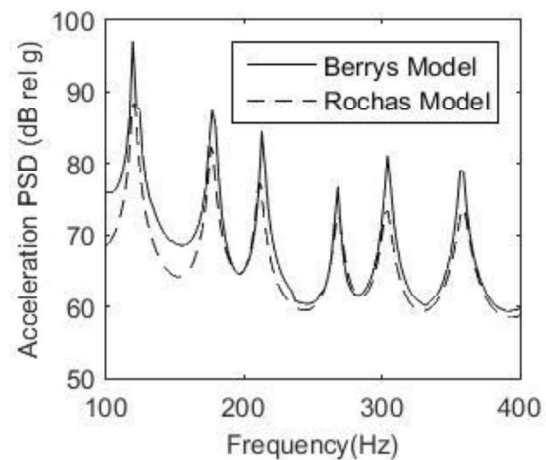


Figure 6: Comparison of acceleration PSD results for a panel with simply supported boundary conditions at a point $x=a/4$ and $y=b/4$ with a TBL excitation applied.

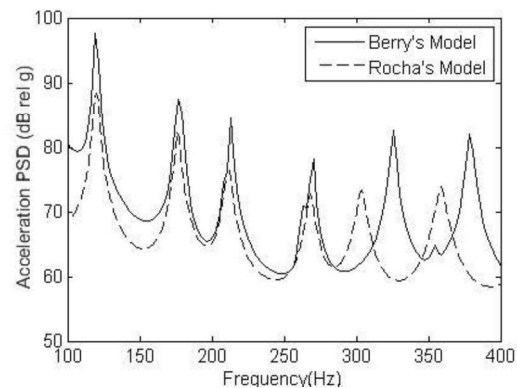


Figure 7: Comparison of acceleration PSD results for a panel with simply supported boundary conditions at a point $x=a/4$ and $y=b/4$, with a TBL excitation applied. Each target frequency is calculated with the same constant number of panel modes $(m, n) = (9, 7)$.

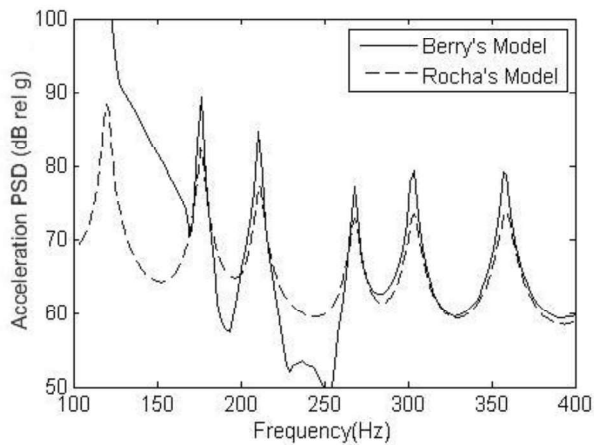


Figure 8: Comparison of acceleration PSD results for a panel with simply supported boundary conditions at a point $x=a/4$ and $y=b/4$, with a TBL excitation applied. Each target frequency is calculated with the same constant number of panel modes $(m,n) = (14,11)$.

Currently, in order to match Berry's model to Rocha's model, a trial and error approach is required to determine the number of panel modes used at each frequency. In order to get the results in Figure 6, the convergence test was used to calculate the number of panel modes needed, however, five times the target frequency was used as the input to the test in Berry's model.

3.3 Piezoelectric patch excitation

A piezoelectric patch has been attached to the test panel using double sided tape. This method is not as accurate as bonding it with glue, however, it allows for the patch to be moved and multiple tests to be run. The double sided tape has not proven to have a large impact on the results as can be seen from Figure 9. The piezoelectric patch is given a frequency sweep with a constant voltage swing and the acceleration measurements taken. Table 3 contains the parameters of the piezoelectric patch used to excite the panel. Using Charrete and Berry's piezo model for a piezoelectric patch on a panel with arbitrary boundary conditions, the acceleration PSD has been predicted and compared to the experimental data obtained at DLR by the authors. The comparison between the predicted response and the actual response is shown in Figure 9. Three other patches and accelerometer configurations have been tested and exhibit similar results. The locations of these tests on the panel can be seen in **Erreur ! Source du renvoi introuvable.**

Figure 9 shows that the model predicts the panel response between 100 and 400 Hz. Below 100 Hz the mounting structure adds additional natural frequencies. This is why below 100 Hz the predicted model does not appear to give good results because it is the natural frequencies of the support structure that is being obtained. Also, above 400 Hz the polynomial spatial functions do not provide accurate results due to matrices appearing singular. The polynomial spatial functions at high modal numbers start to approach infinity at an exponential rate. The division by such a matrix causes the solution to appear singular. This means the

prediction becomes less accurate as the modal number increases. The 400 Hz limiting frequency could be increased if the thickness of the panel is increased. However between the 100 and 400 Hz range the model appears to accurately predict the panels' response due to the piezoelectric patch excitation.

4 Conclusions

The objective of the present study is to validate models of an aircraft panel given different excitations on the panel. The models were given a point force excitation from an impact hammer, a turbulent boundary layer excitation caused by the flow on the outside of the panel, and an excitation from a piezoelectric actuator bonded to the panel. The theoretical values, as predicted by the models, are validated against experimental data from the three excitations. The models were modified to incorporate each of the excitations.

Rocha's model has previously been validated against experimental data. In this work, Rocha's model and Berry's model for a panel with simply supported boundary conditions, and the two models appear to agree for a range of frequencies (mostly low frequencies) for the different excitations. In order to study panels with arbitrary boundary conditions, Berry's model was considered for an optimization routine. The model has been modified using Rocha's power spectral density approach, and has been shown that Berry's modified model can be used to accurately predict a panel's acceleration PSD given a point force excitation, a TBL excitation and a piezoelectric patch excitation over a limited frequency range. Berry's current model has been found to only be valid for a finite number of panel modes due to the polynomial spatial functions. In the future, other spatial functions might be of interest to test to determine if a function exists that does not limit the frequency range as substantially. The different excitations have been validated against Ansys, Rocha's model and experimental data.

Since Berry's modified model has been proven to give an accurate prediction of the acceleration PSD, over a limited frequency range, for each of the excitations it can now be used to select the optimal positions of piezoelectric patches to reproduce the acceleration PSD caused by a TBL in constant cruise conditions.

Table 3: Piezoelectric patch parameters.

Variable	Description, Units	Value
L_x^{pz}	Length of piezoelectric patch [m]	0.061
L_y^{pz}	Width of piezoelectric patch [m]	0.035
L_z^{pz}	Thickness of piezoelectric patch [m]	0.0002
ρ_{pz}	Density of piezoelectric patch [kg m ⁻³]	7500
e_{31}^{pz}	Effective piezoelectric transverse coefficient (x-direction)	1.02
e_{32}^{pz}	Effective piezoelectric transverse coefficient (y-direction)	1.23
$\Delta\varphi^{pz}$	Applied voltage peak to peak [V]	8.5
V^{pz}	Applied voltage offset [V]	200

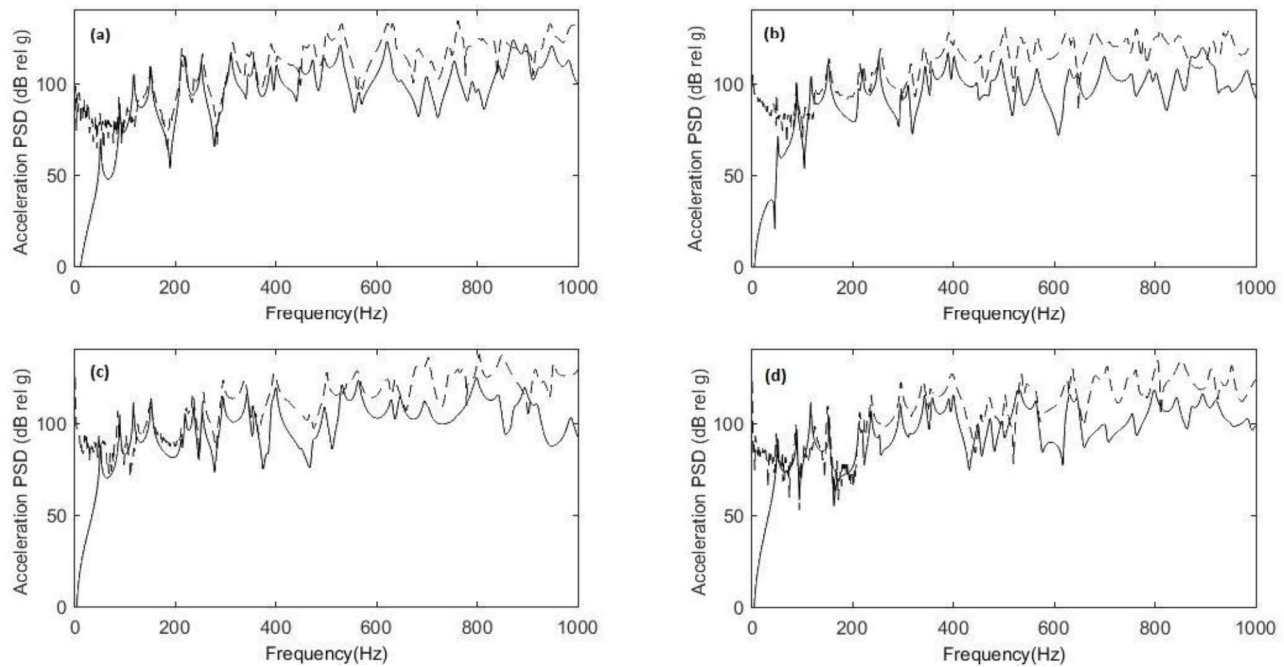


Figure 9: Comparison, using Berry's model, of predicted (solid line) vs. experimental (dashed line) of acceleration PSD results for a panel with arbitrary boundary conditions: (a) measured at (M): $x = 26.2$ cm, $y = 8.6$ cm with a piezoelectric actuator excitation applied at (F): $x = 12.3$ cm, $y = 7.4$ cm (b) M: $x = 31.4$ cm, $y = 26.0$ cm and F: $x = 12.3$ cm, $y = 7.4$ cm (c) M: $x = 31.4$ cm, $y = 26.0$ cm and F: $x = 15.5$ cm, $y = 26.0$ cm (d) M: $x = 25.5$ cm, $y = 13.4$ cm and F: $x = 15.5$ cm, $y = 26.0$ cm

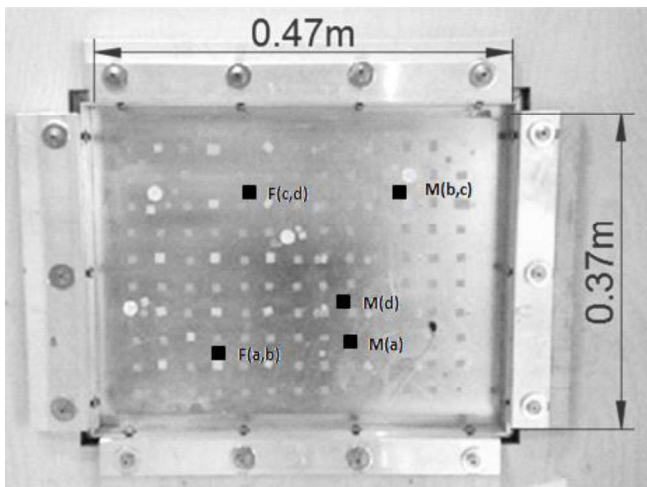


Figure 10: Front view of the DLR test setup with piezoelectric actuator excitation test locations.

This would allow for cost intensive flight and wind tunnel tests to be reduced and replaced by ground tests using a simple panel/piezoelectric patch experimental setup.

Acknowledgements

This work was supported by the Natural Sciences and Engineering Research Council, Carleton University, Deutsches Zentrum für Luft- und Raumfahrt, the German Aerospace Center, Institute of Composite Structures and Adaptive Systems.

References

- [1] J. Rocha, A. Suleman, F. Lau, An accurate Coupled Structural-Acoustic Analytical Framework for the Prediction of Random and Flow-Induced Noise in Transport Vehicles: Its Validation, *Can. Acoust.* 37 (2009).
- [2] W.A. Strawderman, R.S. Brand, Turbulent-flow-excited vibration of a simply supported, rectangular plate, *J. Acoust. Soc. Am.* 45 (1969) 177–192.
- [3] C. Maury, P. Gardonio, S.J. Elliot, A number approach to modelling the response of a randomly excited panel, part i: General theory, *J. Sound Vib.* 252 (2002) 83–113.
- [4] C. Maury, P. Gardonio, S.J. Elliot, A wavenumber approach to modelling the response of a randomly excited panel, part ii: Application to aircraft panels excited by a turbulent boundary layer, *J. Sound Vib.* 252 (2002) 115–139.
- [5] N.H. Schiller, Decentralized control of sound radiation from periodically stiffened panels, Virginia Polytechnic Institute and State University, Blacksburg, Virginia, 2007.
- [6] J.M. Montgomery, Modelling of aircraft structural-acoustic response to complex sources using coupled fem-bem analyses, *Collect. Tech. Pap. - 10th AIAA/CEAS Aeroacoustics Conf.* 1 (2004) 266–274.
- [7] N. Roy, M. Lapi, Efficient Computation of the Radiated Sound Power of Vibrating Structures using a Modal Approach, in: *Acoustics, Paris, 2008*: pp. 381–386.
- [8] J. Rocha, D. Palumbo, On the Sensitivity of Sound Power Radiated by Aircraft Panels to Turbulent Boundary Layer Parameters, *J. Sound Vib.* 331 (2012) 4785–4806.
- [9] J. Rocha, Sound Radiation and Vibration of Composite Panels Excited by Turbulent Flow: Analytical Prediction and Analysis, *Shock Vib.* 2014 (2014) 1–18.

[10] J. Rocha, A. Suleman, F. Lau, Turbulent Boundary Layer Induced Noise and Vibration of a Multi-Panel Walled Acoustic Enclosure, *Can. Acoust.* 38 (2010) 9–22.

[11] J. Rocha, A. Suleman, F. Lau, Prediction of Turbulent Boundary Layer Induced Noise in the Cabin of a BWB Aircraft, *Shock Vib.* 19 (2012) 693–705.

[12] A. Berry, J.-L. Guyader, J. Nicolas, A general formulation for the sound radiation from rectangular, baffled plates with arbitrary boundary conditions, *J. Acoust. Soc. Am.* 88 (1990) 2792–2802.

[13] C. Maury, S.J. Elliot, P. Gardonio, Turbulent boundary-layer simulation with an array of loudspeakers, *AIAA J.* 42 (2004) 706–713.

[14] S.J. Elliot, C. Maury, P. Gardonio, The synthesis of spatially correlated random pressure fields, *J. Acoust. Soc. Am.* 117 (2005) 1186–1201.

[15] T. Bravo, C. Maury, The experimental synthesis of random pressure fields: Methodology, *J. Acoust. Soc. Am.* 120 (2006) 2702–2711.

[16] C. Maury, T. Bravo, The experimental synthesis of random pressure fields: Practical feasibility, *J. Acoust. Soc. Am.* 120 (2006) 2712–2723.

[17] M. Aucejo, L. Maxit, J.-L. Guyader, Experimental simulation of turbulent boundary layer induced vibrations by using a synthetic array, *J. Sound Vib.* 331 (2012) 3824–3843.

[18] O. Robin, A. Berry, S. Moreau, Experimental vibroacoustic testing of plane panels using synthesized random pressure fields, *J. Acoust. Soc. Am.* 135 (2014) 3434–3445.

[19] M. Misol, S. Algermissen, N. Hu, P. Monner, H. Measurement, simulation and synthesis of turbulent-boundary-layer-induced vibrations of panel structures, in: *Proc. 23rd Int. Congr. Sound Vib.*, 2016.

[20] T. Bravo, C. Maury, A synthesis approach for reproducing the response of aircraft panels to a turbulent boundary layer excitation, *J. Acoust. Soc. Am.* 129 (2011) 143–153.

[21] J. Ochs, J. Snowdon, Transmissibility across simply supported thin plates. I. Rectangular and square plates with and without damping layers., *J. Acoust. Soc. Am.* 58 (1975) 832–840.

[22] Y. Champoux, S. Brunet, A. Berry, Champoux, Y, *Exp. Tech.* 20 (1996) 24–26.

[23] W. Hoppmann, J. Greenspon, An experimental device for obtaining elastic rotational constraints on the boundary of a plate, in: *Natl. Congr. Appl. Mech.*, 1954: pp. 14–18.

[24] A. Barnard, S. Hambric, Development of a set of structural acoustic teaching demonstrations using a simply-supported panel., in: *Noise-Con*, 2014: pp. 8–10.

[25] O. Robin, J. Chazot, R. Boulandet, M. Michau, A. Berry, A. Noureddine, A plane and thin panel with representative simply supported boundary conditions for laboratory vibroacoustic tests, *Acta Acust. United with Acust.* 102 (2016) 1–13.

[26] N. Hu, M. Misol, Effects of riblet surfaces on boundary-layer-induced surface pressure fluctuations and surface vibration, in: *Dtsch. Jahrestagung Fur Akust. Deutsche Gesellschaft Fur Akust.*, 2015: pp. 1–4.

[27] F. Charette, F. Berry, C. Guigou, Dynamic Effects of Piezoelectric Actuators on the Vibrational Response of a Plate, *J. Intell. Mater. Syst. Struct.* 8 (1997) 513–524.

[28] G. Corcos, Resolution of pressure in turbulence, *J. Acoust. Soc. Am.* 35 (1963) 192–199.

[29] D.M. Efimtsov, Characteristics of the field of turbulent wall pressure fluctuations at large Reynolds numbers, *Sov. Phys. Acoust.* 28 (1982) 289–292.

[30] S.A.J. Sonnenberg, J. Rocha, Optimization study and panel parameter study for noise radiation reduction of an aircraft panel excited by turbulent flow, *J. Can. Acoust.* 44 (2016) 256–257.

Nomenclature

a	Panel Length [m]
b	Panel Width [m]
D_p	Panel Bending Stiffness [N m]
D_{pp}	Damping Matrix (Rocha's Model)
E_p	Panel Elasticity Modulus [Pa]
f_{mn}	Force Function Matrix based on the excitation
h_p	Panel Thickness [m]
\tilde{K}_{mnpq}	Complex Stiffness Matrix (Berry's Model)
K_{pp}	Stiffness Matrix (Rocha's Model)
m_x, m_y	Plate Mode
M	Total Number of Plate Modes Considered
M_{mnpq}	Mass Matrix (Berry's Model)
M_{pp}	Mass Matrix (Rocha's Model)
N_x	Panel Longitudinal Tension [N m ⁻¹]
N_y	Panel Lateral Tension [N m ⁻¹]
$S_{ref}(\omega)$	Efimtsov's model of the TBL pressure spectrum
ρ_p	Panel Density [kg m ⁻³]
ν_p	Poisson Ratio
ζ_p	Damping Ratio

Appendix A – Rocha's model details

The first step to calculating the acceleration PSD is to determine the panel modes and the natural frequency that corresponds with each mode, as follows [10]:

$$\omega_{m_x m_y}^p = \sqrt{\frac{1}{\rho_p h_p} \left\{ D_p \left[\left(\frac{m_x \pi}{a} \right)^2 + \left(\frac{m_y \pi}{b} \right)^2 \right]^2 + N_x \left(\frac{m_x \pi}{a} \right)^2 + N_y \left(\frac{m_y \pi}{b} \right)^2 \right\}} \quad (34)$$

Where:

$$D_p = \frac{E_p h_p^3}{12(1 - \nu_p^2)} \quad (35)$$

This equation can be simplified to assume that the panel is not under tension ($N_x = N_y = 0$) in either direction. This simplified equation can be seen below [10]:

$$\omega_{m_x m_y}^p = \sqrt{\frac{D_p}{\rho_p h_p} \left[\left(\frac{m_x \pi}{a} \right)^2 + \left(\frac{m_y \pi}{b} \right)^2 \right]} \quad (36)$$

In order to determine how many modes are needed at a specific frequency, a convergence test must be completed. Convergence is reached when the distance between two nodes of the structural mode shape is less than or equal to one half-wavelength, $\lambda/2$, of the bending wave on the plate at the analysis frequency [10]. These values must be rounded to the next highest whole number, to coincide with a plate modal number [10]:

$$N_{Max} = \frac{2a}{\lambda}; M_{Max} = \frac{2b}{\lambda}; \quad (37)$$

$$\lambda = 2\pi \left(\frac{D_p h_p}{\rho_p} \right)^{0.25} (\omega)^{-0.5}$$

The convergence test determines the point at which additional panel modes do not change the overall shape of

the final plot, but instead, appear to make the plot slightly noisier. By running a convergence test at every target frequency, it allows the program to limit the number of panel modes used for lower target frequencies, speeding up the computational time to run the program.

Equation (3) can also be arranged as follows to better show how it can be reduced to equation (4) [1]:

$$Y(\omega) = H(\omega)X(\omega) \quad (38)$$

$$Y(\omega) = \begin{Bmatrix} W(\omega) \\ P(\omega) \end{Bmatrix} \quad (39)$$

$$X(\omega) = \begin{Bmatrix} P_{tbl}(\omega) \\ 0 \end{Bmatrix} \quad (40)$$

$$H(\omega) = \begin{bmatrix} -\omega^2 M_{pp} + i\omega D_{pp} + K_{pp} & K_{pc} \\ -\omega^2 M_{cp} & -\omega^2 M_{cc} + i\omega D_{cc} + K_{cc} \end{bmatrix}^{-1} \quad (41)$$

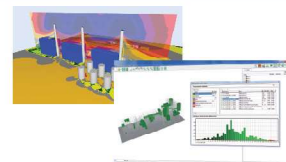
Sound and Vibration Instrumentation *Scantek, Inc.*



Sound Level Meters
Selection of sound level meters for simple noise level measurements or advanced acoustical analysis



Vibration Meters
Vibration meters for measuring overall vibration levels, simple to advanced FFT analysis and human exposure to vibration



Prediction Software
Software for prediction of environmental noise, building insulation and room acoustics using the latest standards



Building Acoustics
Systems for airborne sound transmission, impact insulation, STIPA, reverberation and other room acoustics measurements



Sound Localization
Near field or far field sound localization and identification using Norsonic's state of the art acoustic camera



Monitoring
Temporary or permanent remote monitoring of noise or vibration levels with notifications of exceeded limits

Scantek, Inc.
Sales, Rental, Calibration

www.ScantekInc.com 800-224-3813



Don't miss your **TARGET**

Simply put, poor tuning equals poor masking. In fact, each decibel decrease in overall volume can reduce performance by 10%. Failing in just one key frequency can reduce it by 5%. LogiSon TARGET rapidly adjusts the masking sound to meet the specified spectrum with unequaled accuracy, reducing tuning time while maximizing benefits.

logison.com

© 2018 K.R. Moeller Associates Ltd. LogiSon is a registered trademark of 777388 Ontario Limited.



LogiSon[®]
ACOUSTIC NETWORK